A Novel Physics-informed Framework for Real-time Adaptive Modal Parameters Estimation of Offshore Structures

Fushun Liu[a,b,*], Qianxiang Yu[a], Hong Song[a], Xingguo Li[a], Lihua Liu[a], Dianzi Liu[c]

[a] *College of Engineering, Ocean University of China, Qingdao 266100, China*
[b] *Shandong Province Key Laboratory of Ocean Engineering, Ocean University of China, Qingdao 266100, China*
[c] *School of Engineering, University of East Anglia, Norwich, NR14 7TH, United Kingdom*

Abstract

Singular value decomposition provides a rigorous mathematical foundation for these monitoring methods, such as modal analysis, damage detection, etc. As substantial limitations including computational efficiency and adaptive capabilities have been identified in the matrix process, data-driven algorithms with enhanced efficiency and accuracy to adapt the rapid development of information and technologies have been highly required in offshore structures monitoring. To meet this demand, a novel physics-informed frame work enabling the real-time adaptive monitoring has been proposed in this paper. The working principle of the developed framework has been represented by the smart conversion of physics-informed modal identification into the optimal process of fast and accurate solving an eigensystem governed by differential equations via recurrent neural network. The ingenious design of the proposed framework has complied with the rule of singular value decomposition used for modal identification and therefore, learning capabilities of the physics-informed framework have been remarkably enhanced by successfully addressing two bottleneck problems including proper initialized input values and the optimal time increment of the developed recurrent neural network. Both numerical simulations and the field-data based study of a mono-pile offshore wind turbine structure have been presented to examine the superior performance of the proposed framework. Results have shown that the proposed framework has the ability to adaptively identify modal parameters with a higher level of computational efficiency as compared with traditional methods. Furthermore, the computational advantage of the develop framework has demonstrated the potential to integrate with sensor networks and edge computing for smart monitoring and maintenance in various engineering subjects.

Keywords:

Offshore structures; Singular value decomposition; Physics-informed; Adaptive modal identification; Recurrent neural network;

1. Introduction

Machine learning (ML) techniques have demonstrated the powerful ability to conduct analysis, prediction, diagnosis and other mathematically formulated experiments arising from a broad range of engineering and science projects. With the rapid development of information and sensing technologies, ML has been extensively employed to solve the problems in the areas of structural health monitoring and safety assessment by researchers in the last few decades. To realize adaptive capabilities, distributed edge computing and adaptive identification for real-time health monitoring, big-data analysis-based ML techniques have been used to assist modal analysis, data anomaly identification (Ahmad et al., 2017, Erhan et al., 2021, Mao et al., 2020), structural damage monitoring and detection (Avci et al., 2021, Feijo et al., 2021, Puruncajas et al., 2020, Yao et al., 2019), life evaluation and prediction (Weijtjens et al., 2016), etc., leveraging to their advantages in intelligent optimization, non-linear expression, data modelling, and fast execution (Flah et al., 2021, Lei et al., 2022, Lu et al., 2018, Yuan et al., 2020).

In the long-term service life, the potential fatigue or damage of offshore structures, such as offshore wind turbine (OWT) and platforms can be caused by environmental and operational loadings, leading to the changes in modal parameters. Therefore, the real-time and adaptive monitoring is essential for offshore structures safely operating in complex ocean environment, such as modal analysis, damage detection, etc. Benefiting from advances in modal analysis technology, the operational modal analysis (OMA) method has become more popular and extensively applied in offshore engineering practices. It enables the extraction of modal parameters based on measuring the responses of offshore structures under the ambient or operational excitation that is not required to be measured (Bao and Shi, 2019, Dong et al., 2018, Zhou et al., 2019). To achieve reliable inspections of structures and maintain the serviceability at acceptable levels, the improved demand on self-autonomy of modal identification has been an emerging challenge in the field of structural health monitoring. Many researchers have been working on the realization of more adaptive modal analysis methods using ML technologies. Devriendt et al. (Devriendt et al., 2014) combined the traditional stability diagram with data clustering algorithm to realize the automatic modal identification of a mono-pile offshore wind turbine structure. Su et al. (Su et al., 2020) applied the uncertainty map method to

*Corresponding author.
Email address: percyliu@ouc.edu.cn (Fushun Liu)

achieve the autonomous identification of modal parameters using the convolutional neural network (CNN) image recognition algorithm and solved the problems including the large computational complexity and manual dependence on the stability graph. Torbol et al. (Torbol and Park, 2018) introduced an innovative non-contact sensing technique for vision-based displacement measurement using the K-means clustering algorithm to identify structure modal parameters. Worden et al. (Worden and Green, 2017) demonstrated a data-based approach motivated by Shaw-Pierre method to exploit the non-linear modal analysis. Olivier et al. (Olivieri et al., 2020) developed an online modal parameters identification system to exploit the frequency measurements obtained from actual PMU devices by a ML approach with offline training. Meanwhile, many researchers have tried to obtain modal parameters directly by neural networks. Qin et al. (Qin et al., 2021) proposed a new parameter identification method under non-white noise excitation using the transformer encoder and long short-term memory networks (LSTMs) and applied the random decrement technique (RDT) to preprocess the noised input data. Fang et al. (Fang et al., 2017) developed an unsupervised-learning CNN to identify the modal parameters only from acceleration signals. In general, it is difficult to directly apply neural networks to precisely identify modal parameters because of the specific physical constraints between modalities, which obstruct the network convergence to the expected modal characteristics. For many cases related to physical system modellings, there are a lot of prior knowledge hidden in the response data. These rules can act as a regularization agent in the network to limit the space of admissible solutions to a manageable size. Inspired by the physics-informed learning models, Facchini et al. (Facchini et al., 2014) defined a feed-forward back-propagation (FFBP) network which was fed with four frequency-dependent indicators based on specific properties of the spectral tensor extracted from vibration measurements, and applied this network to assess structural eigenvalues and eigenmodes. Bao et al. (Bao and Li, 2020) proposed a self-coding deep neural network using a novel loss function to constrain the independent feature under the consideration of uncorrelated and non-Gaussian relationship between each modal component for the realization of structural modal parameters.

Taking into account the aforementioned situations, the ML techniques can provide a feasible and effective approaches to realize a more adaptive modal analysis for health monitoring of offshore structures and further implemented in the structural performance evaluation, such as fatigue analyses (Liao et al., 2022) and reliability analyses (Luo et al., 2022a,b, Teng et al., 2022). What's more, the neural network-based modal identification can achieve a more convincing modal identification using prior physical knowledge than the methods simply implemented by neural networks. Therefore, a novel physics-informed framework

enabling the real-time adaptive performance monitoring has been proposed and verified by an in-service OWT structure in this paper to realize a more efficient and accurate modal parameters extraction from structural vibration responses. The ingenious design of the proposed framework has complied with the rule of singular value decomposition (SVD) used for modal parameters identification by the smart conversion of physics-informed modal identification into the optimal process of fast and accurate solving a set of differential equations via a novel designed recurrent neural network (RNN). It should be noted that the proposed RNN-SVD is rigorously governed by the differential equations following the recurrent calculation process, whilst the traditional RNN is a data-driven method without the guidance of mathematical or physical knowledge in post-propagation updating, causing the gradient vanishing, high computational cost, etc.(Choe et al., 2021, Qiu et al., 2020, Schmidt, 2019) Therefore, the computational complexity of SVD has been effectively reduced, leading to its more applications in embedding systems and edge computations. Meanwhile, considering the changeable external load conditions in practical offshore engineering problems, a data pattern matching mechanism has been implemented into the proposed framework to adaptively determine the network hyper-parameters throughout the offline pre-training process. Following that, numerical examples have been examined to demonstrate the correctness and effectiveness of the developed physics-informed network in terms of the time step and initial conditions. To further prove the ability of the proposed framework on real-time modal monitoring under time-varying external conditions, a vibration response dataset of an in-service OWT structure subject to different operational environments has been tested.

2. Methodology

SVD is a mathematical representation for general matrices used in many modal analysis methods such as stochastic subspace identification (SSI) (Peeters and De Roeck, 1999), eigensystem realization algorithm (ERA) (Ibrahim and Mikulcik, 1977, James et al., 1995, Juang and Pappa, 1985), Pole-residues method (Liu et al., 2016, Zhou et al., 2019) etc. which are an important class of OMA algorithms and have been extensively developed in the field of structural health monitoring. The common principle for the aforementioned methods is to establish the mathematical model of the system representing the relationship between the structural response and system eigenvalues for the identification of modal parameters. In order to realize a more adaptive and efficient modal identification method, the proposed framework has replaced the traditional SVD used in these methods with a RNN to effectively reduce the calculation complexity for real-time structural monitoring. Meanwhile, the pre-training mechanism has been implemented into the

framework by the mapping of structural responses to the specific data pattern prior to modal identification in order to enable the framework with the more adaptability to offshore structures subject to different external loadings. To demonstrate the proposed physics-informed modal identification framework leveraging the working principle of SVD-based methods, the Pole-residues method as an example of signal decomposition technique for singular values, has been briefly introduced as follows. For simplicity, the standard notation has been applied throughout the paper: The lowercase letter, bold lowercase letter and bold uppercase letter represent the scalar, vector and matrix, respectively.

2.1. Principle of the Pole-residues method

The transfer function in the Pole-residues method provides a foundation to determine key characteristics of the system response using poles and zeros, instead of solving the complex differential equation. In the digital signal analysis, a discrete structural response signal y_k in finite time steps can be formulated in a Pole-residues form shown in Eq. (1):

$$y_k \equiv y(t_k) = \sum_{n=1}^{L} r_n e^{\lambda_n k \Delta t} \tag{1}$$

where y_k encompasses a complex series of components. λ_n and r_n are poles and residues of the n^{th} component, respectively. λ_n is expressed in the form of $\lambda_n = -\alpha_n + j\omega_n$, α_n represents the damping factor and ω_n means the frequency in radians, $j = \sqrt{-1}$. Δt denotes the finite time step and $t_k = k\Delta t$.

The structural response can be determined by a Hankel matrix $\mathbf{H}(k)$ that is defined as:

$$\mathbf{H}(k) = \begin{bmatrix} y_k & y_{k+1} & \cdots & y_{k+\eta-1} \\ y_{k+1} & y_{k+2} & \cdots & y_{k+\eta} \\ \vdots & \vdots & \ddots & \vdots \\ y_{k+\xi-1} & y_{k+\xi} & \cdots & y_{k+\xi+\eta-1} \end{bmatrix} \tag{2}$$

where ξ and η represent the selected row and column of $\mathbf{H}(k)$. Then, substituting $k = 0$ into Eq. (2) and applying the SVD:

$$\mathbf{H}(\mathbf{0}) = \begin{bmatrix} \mathbf{U}_1 & \mathbf{U}_2 \end{bmatrix} \begin{bmatrix} \mathbf{S}_1 & \mathbf{0} \\ \mathbf{0} & \mathbf{0} \end{bmatrix} \begin{bmatrix} \mathbf{V}_1^\top \\ \mathbf{V}_2^\top \end{bmatrix} = \mathbf{U}_1 \mathbf{S}_1 \mathbf{V}_1^\top \tag{3}$$

where the superscript $\top$ denotes the matrix transpose.

Note that the $\mathbf{H}(k)$ can be expressed as the product of three matrices: $\mathbf{H}(k) = \boldsymbol{\mathcal{P}}_\xi \mathbf{A}^k \boldsymbol{\mathcal{Q}}_\eta$, where $\boldsymbol{\mathcal{P}}_{\boldsymbol{\xi}}$ is the observability matrix, $\boldsymbol{\mathcal{Q}}_{\boldsymbol{\eta}}$ is the controllability matrix and $\mathbf{A}$ is the system matrix (Lam and Mevel,

2011). Then, the $\mathbf{H}(0)$ and $\mathbf{H}(1)$ yield:

$$\mathbf{H}(0) = \boldsymbol{\mathcal{P}}_{\xi}\boldsymbol{\mathcal{Q}}_{\eta} \tag{4}$$

$$\mathbf{H}(1) = \boldsymbol{\mathcal{P}}_{\xi}\mathbf{A}\boldsymbol{\mathcal{Q}}_{\eta} \tag{5}$$

The comparison of Eqs. (3) and (4) suggests a "possible balanced choice" (Hu et al., 2013): $\boldsymbol{\mathcal{P}}_{\xi} = \mathbf{U}_1\mathbf{S}_1^{1/2}$ and $\boldsymbol{\mathcal{Q}}_{\eta} = \mathbf{S}_1^{1/2}\mathbf{V}_1^{\top}$, so the Eq. (5) can be reformulated as Eq. (6):

$$\mathbf{H}(1) = \mathbf{U}_1\mathbf{S}_1^{1/2}\mathbf{A}\mathbf{S}_1^{1/2}\mathbf{V}_1^{\top} \tag{6}$$

Thus, the realization of the system matrix $\mathbf{A}$ is achieved by Eq. (7) below:

$$\mathbf{A} = \mathbf{S}_1^{-1/2}\mathbf{U}_1^{\top}\mathbf{H}(1)\mathbf{V}_1\mathbf{S}_1^{-1/2} \tag{7}$$

For more details about solving Eq. (1) with a stable numerical solution, see Hu (Hu et al., 2013). Usually, the poles λ_n can be formulated as a function of the eigenvalues z_n of the system matrix $\mathbf{A}$: $\lambda_n = ln(z_n)/\Delta t$. Substituting the calculated λ_n into Eq. (1), the residues r_n can be obtained using the linear least square method.

The aforementioned principle enables the Pole-residues method a powerful tool for modal analysis of structures subject to arbitrary external excitations. However, in the practical engineering, the following three deficiencies greatly limit the application of these methods for online modal monitoring:

1) The complexity of traditional SVD in the computation process is increased with the order of $\mathcal{O}(\mathcal{N}^{\ni})$ ($\mathcal{N}$ means the dimension of Hankel matrix);

2) The dimension of response matrix needs to be determined based on much experience and prior knowledge;

3) There is no standard guidance for the model order estimation which needs to be adapted to the time-varying environment in real-time monitoring.

To overcome the above limitations, a physics-informed framework with higher computational efficiency and better adaption to the real-time monitoring has been proposed in the following section.

2.2. Physics-informed framework

To achieve the higher efficiency and more adaptive modal identification, a physics-informed framework has been proposed to solve an eigensystem governed by differential equations using RNN. The developed

framework aims at achieving two features: 1) the advantages of traditional OMA methods should be maximally inherited to enable the designed network encompassing the physical principle-based information by strict mathematical constraints; 2) the measured field-data based on different operational conditions should be adaptively recognized by its pattern for the determination of appropriate hyper-parameters, such as decomposition orders. Based on these understandings, a RNN with optimized parameter and data-pattern matching ability has been designed to solve modal identification problems arising in the adaptive real-time structural monitoring process.

2.2.1. Singular solution using recurrent network

In modal analysis methods such as ERA method, the SVD process is a key step to obtain the system eigenvalues from the Hankel matrix. However, the expensive computation involved in the SVD refrains the modal analysis techniques from streaming data processing in online monitoring. Researches on the efficient realization of SVD have been paid attention by many scholars, such as Feng (Feng et al., 1995), Oja (Oja, 1982), Cichocki (Cichocki, 2002) etc. Based on the understanding of the SVD decomposition process assimilated into the solution to an eigensystem governed by differential equations, Feng (Feng et al., 1995) proposed a combination of the first principal component analysis with $anti-Hebb$ rules to iteratively extract the singular values and their corresponding left and right singular vectors. Thus, the process of SVD is converted into the problem of solving non-linear differential equations which have been defined by Eqs. (8 - 10):

$$\frac{d\mathbf{p}_j(t)}{dt} = \delta_a(\mathbf{G}_j\mathbf{q}_j(t) - \|\mathbf{p}_j(t)\|_2^2\,\mathbf{p}_j(t)) \qquad j = 1, 2, \cdots, M; \tag{8}$$

$$\frac{d\mathbf{q}_j(t)}{dt} = \delta_b(\mathbf{G}_j^\top\mathbf{p}_j(t) - \|\mathbf{q}_j(t)\|_2^2\,\mathbf{q}_j(t)) \qquad j = 1, 2, \cdots, M; \tag{9}$$

$$\mathbf{G}_j = \begin{cases} \mathbf{G}, & j = 1 \\ \mathbf{G} - \mathbf{l}_j\sigma_j\mathbf{r}_j, & others \end{cases} \tag{10}$$

where $\mathbf{G}$ represents a general matrix with $M \times N(M < N)$ dimensions (it will be replaced by the Hankel matrix $\mathbf{H}(0)$ in Eq. (3) for the modal analysis). δ_a and δ_b are constant coefficients. The subscript j is the order number of singular values (in descending order). The $\mathbf{p}_j$ and $\mathbf{q}_j$ are the given vector variables, $\mathbf{p}_j \in \mathbf{R}^M$, $\mathbf{q}_j \in \mathbf{R}^N$. When t becomes infinite, $(||\mathbf{p}_j||_2^2)^{-1}\mathbf{p}_j \to \pm\mathbf{l}_j$, $(||\mathbf{q}_j||_2^2)^{-1}\mathbf{q}_j \to \pm\mathbf{r}_j$, and $||\mathbf{p}_j||_2^2(||\mathbf{q}_j||_2^2) \to \sigma_j$ that indicates the solutions to Eqs. (8) and (9) reach the balance point in an equilibrium state, where $\mathbf{l}_j$, $\mathbf{r}_j$ and σ_j are the j^{th} left singular vector, right singular vector and corresponding

singular value, respectively. Meanwhile, the loss equations of $\mathbf{G}_j\mathbf{q}_j(\infty) - \|\mathbf{p}_j(\infty)\|_2^2\,\mathbf{p}_j(\infty) = \mathbf{0}$ and $\mathbf{G}_j\mathbf{p}_j^\top(\infty) - \|\mathbf{q}_j(\infty)\|_2^2\,\mathbf{q}_j(\infty) = \mathbf{0}$ are satisfied. Here, the $\mathbf{p}_1(\infty)$ and $\mathbf{q}_1(\infty)$ are called the first principal components. The first principle component rule is explained by Eq. (10) which indicates that each component is independently extracted from $\mathbf{G}$ and the previous component would affect the next one.

It should be noted that the proposed framework in this paper is a recurrent neural network directly constructed by two-dimensional differential equations (Eqs. 8 - 9) for solving the SVD (singular value decomposition) problem, whilst the traditional PINN (physics-informed neural network) focuses on solving partial differential equations. To validate the convergence of Eqs. (8 - 10), Feng etc. (Feng et al., 1997) introduced the energy function defined by Eq. (11):

$$E_j(t) = \mathbf{p}_j^\top(t)\mathbf{G}\mathbf{q}_j(t) - \frac{1}{4}(\|\mathbf{p}_j(t)\|_2^4 + \|\mathbf{q}_j(t)\|_2^4) \tag{11}$$

Following the first principle component rule, the differential equation of the first energy function $E_1(t)$ can be formulated as follows:

$$\begin{aligned}\frac{dE_1(t)}{dt} &= (\frac{d\mathbf{p}_1^\top}{dt})[\mathbf{G}\mathbf{q}_1(t) - \|\mathbf{p}_1(t)\|_2^2\,\mathbf{p}_1(t)] + (\frac{d\mathbf{q}_1}{dt})[\mathbf{p}_1^\top(t)H - \|\mathbf{q}_1(t)\|_2^2\,\mathbf{q}_1^\top(t)] \\ &= \left\|\frac{d\mathbf{p}_1}{dt}\right\|_2^2 + \left\|\frac{d\mathbf{q}_1}{dt}\right\|_2^2 \geq 0\end{aligned} \tag{12}$$

The result of Eq. (12) indicates that the $E_1(t)$ is monotonically increasing, which means the system of Eqs. (8) and (9) would not be convergent until getting to the balance points. Actually, there are totally $M+1$ balance points in the form of $(0,0)$ & $(\sqrt{\sigma_m}\mathbf{l}_m, \sqrt{\sigma_m}\mathbf{r}_m)$ $(m = 1, ..., M)$. And the first non-zero point$(\sqrt{\sigma_1}\mathbf{l}_1, \sqrt{\sigma_1}\mathbf{r}_1)$ is the true and global balance point which is known by employing the *"First Method of Lyapunov"*. Similarly, the second principal component can be obtained using Eqs. (13) and (14):

$$\frac{d\mathbf{p}_2(t)}{dt} = \delta_a(\mathbf{G}_2\mathbf{q}_2(t) - \|\mathbf{p}_2(t)\|_2^2\,\mathbf{p}_1(t)) \tag{13}$$

$$\frac{d\mathbf{q}_2(t)}{dt} = \delta_b(\mathbf{G}_2^\top\mathbf{p}_2(t) - \|\mathbf{q}_2(t)\|_2^2\,\mathbf{q}_1(t)) \tag{14}$$

where $\mathbf{G}_2$ is obtained by Eq.(10):

$$\mathbf{G}_2 = \mathbf{G} - \mathbf{l}_1\sigma_1\mathbf{r}_1 \tag{15}$$

It should be noted that Eq. (10) is a key procedure in the whole recurrent process to lead the system converge to the next global balance point. In Eq. (15), the system matrix $\mathbf{G}$ is updated by eliminating the

first component from the original system matrix. After that, the system of Eqs. (13) and (14) remains M balance points: $(0,0)$ & $(\sqrt{\sigma_m}\mathbf{l}_m, \sqrt{\sigma_m}\mathbf{r}_m)$ $(m = 2, ..., M)$ and the second non-zero point $(\sqrt{\sigma_2}\mathbf{l}_2, \sqrt{\sigma_2}\mathbf{r}_2)$ represents the new global balance point. The reason for the matrix reduction lies in the fact that all principal components are coupled but orthogonalized with each other. The first principle component rule is used to realize the de-orthogonalization each of the component in the recurrent process. Following the above procedures, all singular values (in descend order) and its corresponding left and right vectors of matrix $\mathbf{G}$ can be accurately obtained.

To realize the above process, a linear recurrent neural network has been developed as RNN-SVD shown in Fig. 1. In the network, the linear fully connected (FC) layer is utilized to represent the matrix multiplication operation in Eqs. (8) and (9). The loss function is defined by Eq. (16). And $\mathbf{G}$, $\mathbf{p}_j(0)$, $\mathbf{q}_j(0)$ and $\Delta t_j(0)$ are the inputs of the network. $\mathbf{p}_j(t)$, $\mathbf{q}_j(t)$ and Δt_j are the training parameters of RNN-SVD in the recurrent process. As proved by Eq. (12), the network could be convergent with any non-zeros inputs of $\mathbf{p}_j(0)$ and $\mathbf{q}_j(0)$. Moreover, it should be noted that the PINN uses the loss function to assess the difference before and after the iteration of the physical equation using auto-differential method. The differential equation adopted in this paper is directly transformed into a recurrent neural network, in which the iterative process of solving the SVD is analogous to the convergence process of the loss function defined in the PINN network.

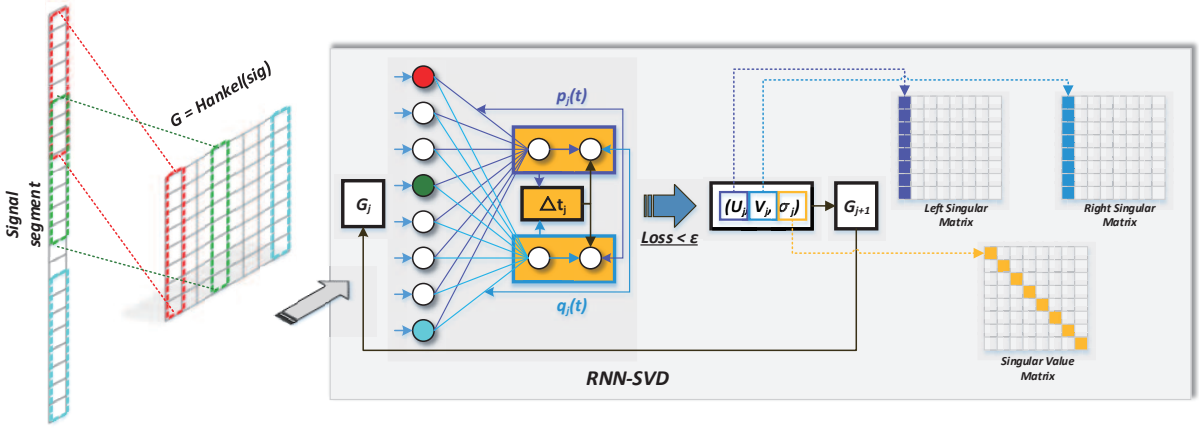

Fig. 1: The proposed RNN-SVD network.

$$Loss = \mathbf{G}_j\mathbf{q}_j(t) - \|\mathbf{p}_j(t)\|_2^2\,\mathbf{p}_j(t) \quad or \quad \mathbf{G}_j\mathbf{p}_j^\top(t) - \|\mathbf{q}_j(t)\|_2^2\,\mathbf{q}_j(t) \tag{16}$$

As mentioned above, the feasibility of the designed RNN on solving singular values has been theoretically proved. To realize a more efficiency modal analysis framework, the advantage on computational ability of the RNN-SVD has to be guaranteed. In the iteration process, there are three parameters determining the efficiency of getting the network to be convergent: time step, $\mathbf{p}_j(0)$ and $\mathbf{q}_j(0)$. More specifically, the time step controls the convergent step length and the $\mathbf{p}_j(0)$ and $\mathbf{q}_j(0)$ determines the distance from the initial value to balanced point. Therefore, both of the initial inputs which is closer to the balanced points and the proper time step would significantly promote the computational efficiency. Generally, the standard SVD can be formulated as Eqs. (17) and (18):

$$\mathbf{G}^\top\mathbf{G} = \mathbf{V}\mathbf{\Sigma}^\top\mathbf{U}^\top\mathbf{U}\mathbf{\Sigma}\mathbf{V}^\top = \mathbf{V}(\mathbf{\Sigma}^\top\mathbf{\Sigma})\mathbf{V}^\top \tag{17}$$

$$\mathbf{G}\mathbf{G}^\top = \mathbf{U}\mathbf{\Sigma}^\top\mathbf{V}^\top\mathbf{V}\mathbf{\Sigma}\mathbf{U}^\top = \mathbf{U}(\mathbf{\Sigma}^\top\mathbf{\Sigma})\mathbf{U}^\top \tag{18}$$

where $\mathbf{U}$ and $\mathbf{V}$ are the eigenvectors of $\mathbf{G}\mathbf{G}^\top$ and $\mathbf{G}^\top\mathbf{G}$, respectively. And $\mathbf{\Sigma}$ is a non-zero singular value diagonal matrix. Conducted by Eqs. (17) and (18), the computational complexity of standard SVD is $\mathcal{O}(\mathcal{N}^\ni)$, more specifically, the decomposition of Hankel matrix ($M \times N$) requires at least $M^3 * 4$ times of multiplications. While, the developed RNN-SVD has just involved the number $M^2 * Iter$ of multiplications, where $Iter$ is the iteration number. Obviously, the iteration number is greatly reduced (i.e. $Iter < 4M$) leading to the considerably improvement of computational efficiency. Therefore, a time-step optimization method and data pattern learning strategy are implemented to set the time step and $\mathbf{p}_j(0)$ and $\mathbf{q}_j(0)$ for realizing an efficient SVD method.

2.2.2. Time step optimization

As described in Section 2.2.1, the time step is one of the important factors for the fast convergent speed to reach the balance point. Eq. (19) presents the discrete process of Eq. (8) about how the time step influences the recurrent process of $\mathbf{p}_j$:

$$\mathbf{p}_j(t+\Delta t) = \delta_a \Delta t(\mathbf{G}_j\mathbf{q}_j(t) - \|\mathbf{p}_j(t)\|_2^2\,\mathbf{p}_j(t)) + \mathbf{p}_j(t) \qquad t = 0, \cdots; \tag{19}$$

In Eq. (19), the speed of convergence depends on two factors including the loss function defined by Eq. (16) and time step (Δt). As the loss is getting smaller in the convergent process, the speed of convergence would be getting slower, leading to more calculations for the converged results. Thus, it is necessary for the time step optimization to accelerate the convergent process. Based on these observations, Eq. (20) has been

provided as the math-based formulation of the time step optimization.

$$\begin{aligned} &\min_{\Delta t_j, Loss} \sum_{j}^{M}(iter_j) \\ &s.t. \quad \begin{cases} \mathbf{G}_j\mathbf{q}_j(t) - \|\mathbf{p}_j(t)\|_2^2\,\mathbf{p}_j(t) & \leq \varepsilon \\ t_j = t_j + \Delta t_j(iter) \end{cases} \end{aligned} \tag{20}$$

where the $iter$ represents the iteration number in the calculation of the j^{th} singular value during the entire process. M is the number of total singular values. The total iteration number is defined as $Iter = \sum_j^M (iter_j)$.

To realize an efficient solution to Eq. (19) via Eq. (20), Eq. (21) has been proposed to remarkably update the Δt in each iteration by the ratio of two losses and a constant exponential index, while the convergent speed would not be significantly reduced with the decrease of the loss function. Therefore, the optimization process is efficiently completed to reach the balanced point for the dynamic system with the minimum effort.

$$\Delta t_j(iter) = (\frac{Loss(iter-1)}{Loss(iter)})^{1/\Delta t_{ratio}(j)} \Delta t_j(iter-1) \qquad iter = 2, \cdots; \tag{21}$$

where $Loss(iter)$ means the loss of the $iter^{th}$ iteration in the network training process defined in Eq. (16). The $\Delta t_{ratio}(j)$ denotes a constant ratio which should be pre-defined to calculate the j^{th} singular value. Δt will be gradually increased with the decrease of the loss during the convergent progress, but its increasing rate is gradually reduced. Therefore, the variable Δt needs to be bounded within a reasonable range to avoid the divergence of results. As $\Delta t_{ratio}(j)$ is adaptively determined by the loss, the upper boundary of Δt is mainly affected by the initial value $\Delta t_j(0)$.

In the practical scenario, the $\Delta t_j(0)$ would be correlated with the response data under different loading conditions. More specifically, the initial parameters of RNN are determined by the singular values of Hankels that are constructed by these responses. In the practical operation and maintenance of OWT, the external loadings regularly vary with wind and rotor speed, which makes it hard to set the initials adaptively. Nevertheless, the wind loading usually performs as a steady stochastic process within a certain time period, indicating a stable structural response pattern. Therefore, the historical response data have been leveraged for the selection of initial values (including $\Delta t_j(0)$, $\mathbf{p}_j(0)$ and $\mathbf{p}_j(0)$). Inspired by this idea, a data pattern learning strategy is implemented into the proposed modal analysis framework to identify the data by feature matching under the similar conditions to realize a more efficient convergent process using the developed network.

2.2.3. *Data pattern matching strategy*

To enable the physics-informed framework with the more adaptability to offshore structures subject to time-varying external loadings during the real-time monitoring process, the data pattern learning algorithm is implemented to distinguish the certain pre-selected pattern from the time-varying field data. Following that, better initial values of inputs could be pre-trained by leveraging the similar data pattern to realize a fast convergence in the SVD process. For OWT structures, the vibration response has divergent performances under different loads such as wind, wave and rotor speed, etc.

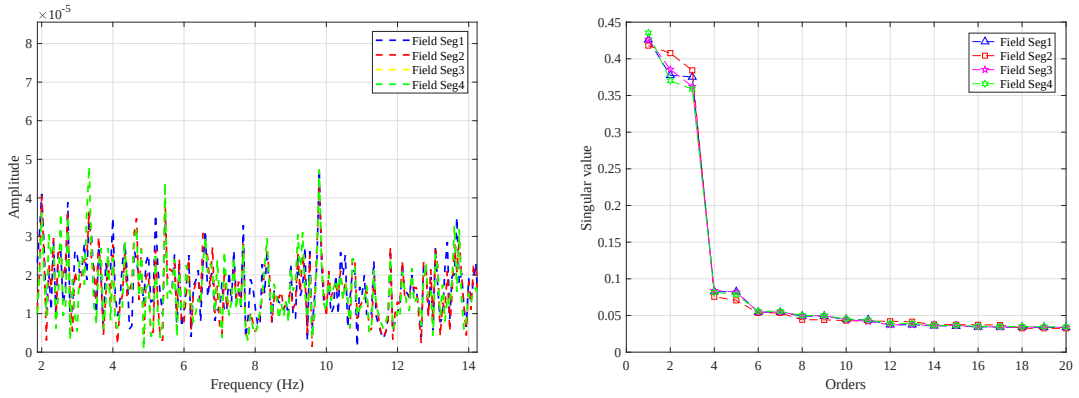

(a) (b)

Fig. 2: The comparison of four segments acceleration data in parking condition: (a) frequency domain, (b) singular values

In the data pattern matching strategy, typical responses need to be selected from a long period monitoring dataset to facilitate the SVD of field measurements with the high level of efficiency. As the impact load is useful for accurate vibration analysis, owing to the most energy of the decomposed modal components, the response induced by strong pulsed loads is preferred. However, this situation does not frequently occur in the normal case. Taking into accounts this situation, the data pattern matching strategy for the identification of operational conditions in the pre-training session is implemented in the proposed framework to realize a more robust and efficient SVD-based monitoring system. First, several representative data patterns are selected from the long-term monitoring dataset. The features represented by these patterns should reflect the shared information on responses under the similar operational conditions such as the parking or operational status of OWT, that is to say, the external loads statistically have the similar distribution with the change of magnitudes in an acceptable perturbation considering the typical working status. In order to effectively measure the compactness between data segments and selected patterns, the *Pearson-correlation*

is applied for pattern identification in the matching process. Mathematically, the singular values are correlated with frequency components of the response signal, thus, the higher correlation in frequency domain means the higher matching index of singular values. As shown in Fig. 2, the data in the similar operational conditions have shared the common features and performances in terms of frequency and singular values, leading to the values of correlation coefficients are over 0.97. In the practical monitoring, the threshold of correlation coefficients should be determined on the basis of the matching degree of the investigated field measurements. It is worth noting that each feature represented by a data pattern should be learned by the network with specific hyper-parameters during the offline pre-training process. Employing the RNN-SVD network and time step optimization, the initial inputs of the selected data patterns, such as $\mathbf{p}_j(0)$, $\mathbf{q}_j(0)$, $\Delta t_j(0)$ etc., are trained by the offline training process. Therefore, once the pattern of monitoring data is determined, the corresponding initial conditions are autonomously selected as inputs of RNN-SVD for SVD with the high-level efficiency. Meanwhile, the model order can also be determined through the pre-training process for the adaptive online monitoring of OWT structure. The pseudo-code for the pre-training and data pattern pre-training and matching strategy has been provided in $Algorithm1$. It is noted that the $\mathbf{S}_{acc}$ is an acceleration segment of structure vibration responses, the $\mathbf{S}_{acc}[t]$ and $\mathbf{S}_{acc}[w]$ represent the response in time and frequency domains, respectively. The $\mathbf{S}_{pat_i}$ means the i^{th} response data pattern and $i = 1, \cdots, d$. The d means the amount of data patterns. $P_{th}(i)$ is the pattern matching threshold value. All the selected data patterns are saved in the $HistoryDataset$. $E_{th}(i,j)$ is the threshold value for loss equations and the subscript "(i,j)" means the j^{th} singular value order of the i^{th} data pattern. What' more, output variables in each step are either on the left of an equal sign or at an arrows tip, while input variables are either on the right of an equal sign or at an arrows base. The initialized and return values are inputs and outputs of the whole function, respectively.

Algorithm 1 Data pattern pre-training & matching

Input initialization:$\mathbf{S}_{acc}[t], \mathbf{S}_{pat_i}[t], P_{th}(i), HistoryDataset[\mathbf{S}_{pat_i}]$

$\mathbf{S}_{acc}[w] \leftarrow \mathbf{S}_{acc}[t], \mathbf{S}_{pat_i}[w] \leftarrow \mathbf{S}_{pat_i}[t]$ (FFT)

for $i = 1 \rightarrow d$ **do**

  $P_i \leftarrow \rho(\mathbf{S}_{acc}[w], \mathbf{S}_{pat_i}[w]) = \frac{E[(\mathbf{S}_{acc}[w]-\mu_{\mathbf{S}_{acc}[w]})((\mathbf{S}_{pat_i}[w]-\mu_{\mathbf{S}_{pat_i}[w]})]}{\sigma_{\mathbf{S}_{acc}[w]}\sigma_{\mathbf{S}_{pat_i}[w]}}$ (Pearson Correlation)

  if then$P_i > P_{th}(i)$

    $P_{index} = i$

    $break$

  end if

9: **end for**

10: $\mathbf{H}_i \leftarrow HankelTransform(S_{acc}[t])$ Eq. (2)

11: $[\mathbf{U}_i, \mathbf{S}_i, \mathbf{V}_i] = \mathbf{SVD}(\mathbf{H}_i)$

12: $\mathbf{p}_{ij}(0) = \sqrt{\mathbf{U}_i[:,j]} * \mathbf{S}_i[j,j]; \mathbf{q}_{ij}(0) = \sqrt{\mathbf{V}_i[:,j]} * \mathbf{S}_i[:,j] \quad j = 1, ..., M$

13: **Pre-training**$(HistoryDataset)$ by repeatedly deploying **RNN-SVD**

14: $[\Delta t_{ij}(0), E_{th}(i,j), \Delta t_{ratio}(i,j)] \leftarrow$ **Pre-training**$(HistoryDataset[P_{index}])$

15: **return** $result : \mathbf{p}_{ij}(0), \mathbf{q}_{ij}(0), \Delta t_{ij}(0), E_{th}(i,j), \Delta t_{ratio}(i,j)$

2.2.4. *Framework configuration*

By the implementation of the time step optimization and data pattern algorithm described in Sections 2.2.2 and 2.2.3 into the initial pre-training session, a more efficient singular decomposition network has been established. Based on the RNN-SVD and Eqs. (6) and (7) for modal analysis, a novel physics-informed modal identification framework has been proposed and its schematic illustration has shown in Fig. 3. The pseudo-code for the realization of the proposed framework has been described in $Algorithm2$.

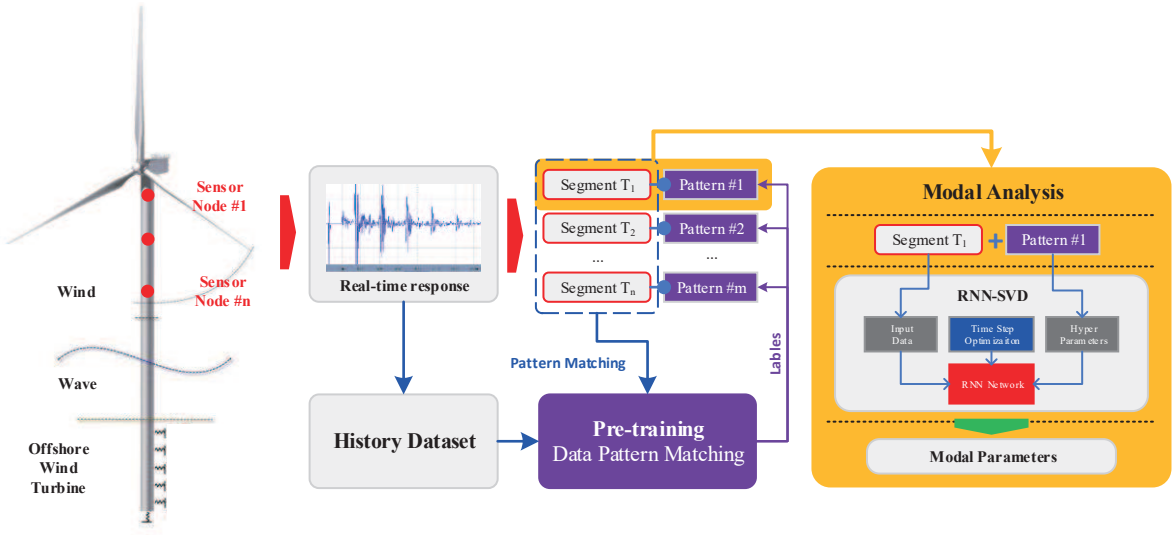

Fig. 3: Schematic illustration of the proposed physics-informed framework.

Algorithm 2 Physical-informed modal analysis framework

1: **function** RNN-SVD$(\mathbf{S}_{acc}, \mathbf{p}_j(0), \mathbf{q}_j(0), \Delta t_j(0), E_{th}(j), \Delta t_{ratio}(j))$

2: $\mathbf{H}_1(0) \leftarrow HankelTransform(\mathbf{S}_{acc}[t])$ Eq. (2)

3: Initializing $\Delta t_j(1) = \Delta t_j(0)$

4: Initializing $\mathbf{p}_j(1), \mathbf{q}_j(1)$ and $Loss(1)$ Eqs. (8, 9, 16)

5: **for** $j = 1 \rightarrow M$ **do**

$iter = 1$

while $Loss(iter) > E_{th}(j)$ **do**

$iter \leftarrow iter + 1$

Update $\mathbf{p}_j(iter)$:

$\mathbf{p}_j(iter) = \Delta t_j(iter-1)(\mathbf{H}_j(0)\mathbf{q}_j(iter-1) - \|\mathbf{p}_j(iter-1)\|_2^2\,\mathbf{p}_j(iter-1)) + \mathbf{p}_j(iter-1)$ Eq. (8)

Update $\mathbf{q}_j(iter)$:

$\mathbf{q}_j(iter) = \Delta t_j(iter-1)(\mathbf{H}_j(0)^\top\mathbf{p}_j(iter-1) - \|\mathbf{q}_j(iter-1)\|_2^2\,\mathbf{q}_j(iter-1)) + \mathbf{q}_j(iter-1)$ Eq. (9)

Update $Loss(iter)$:

$Loss(iter) = \mathbf{G}_j\mathbf{q}_j(iter) - \|\mathbf{p}_j(iter)\|_2^2\,\mathbf{p}_j(iter)$ Eq. (16)

Update $\Delta t_j(iter)$:

$\Delta t_j(iter) = (\frac{Loss(iter-1)}{Loss(iter)})^{1/\Delta t_{ratio}(j)}\Delta t_j(iter-1)$ Eq. (13)

end while

$(||\mathbf{p}_j||_2^2)^{-1}\mathbf{p}_j \rightarrow \pm\mathbf{l}_j$, $(||\mathbf{q}_j||_2^2)^{-1}\mathbf{q}_j \rightarrow \pm\mathbf{r}_j$, and $||\mathbf{p}_j||_2^2/||\mathbf{q}_j||_2^2 \rightarrow \sigma_j$

$\mathbf{U}[:,j] = \mathbf{l}_j, \mathbf{V}[:,j] = \mathbf{r}_j, \mathbf{S}[j,j] = \sigma_j$

$\mathbf{H}_{j+1}(0) = \mathbf{H}_j(0) - \mathbf{l}_j\sigma_j\mathbf{r}_j$ Eq. (10)

end for

return $\mathbf{U}, \mathbf{V}, \mathbf{S}$

end function

---

function MODALPARAMETER($\mathbf{S}_{acc}, \mathbf{U}, \mathbf{V}, \mathbf{S}$)

$\mathbf{H}(1) \leftarrow HankelTransform(\mathbf{S}_{acc}[t])$ Eq. (2)

deploying Eq. (7): $\mathbf{A} = \mathbf{S}^{-1/2}\mathbf{U}^\top\mathbf{H}(1)\mathbf{V}\mathbf{S}^{-1/2}$

$z_n \leftarrow eigen(\mathbf{A})$

$\lambda_n = ln(z_n)/\Delta t$

$f_n = imag(\lambda_n)/(2\pi)$

return $result : f_n$

end function

---

3. Numerical study

In this section, two numerical examples have been studied to demonstrate the accuracy and efficiency of the proposed physics-informed framework for solving an eigensystem governed by differential equations, which will be further used to achieve the real-time adaptive performance monitoring of OWT structures. As discussed on the design of RNN-SVD in Section 2.2.3, there are two most prominent factors including the initial inputs and the time step influencing the convergent speed, to be investigated for the improved overall performance of RNN-SVD.

3.1. General matrix validation

$$\mathbf{G} = \begin{bmatrix} 1.0 & 2.1 & 3.2 & 1.2 \\ 1.3 & 2.1 & 4.0 & 6.0 \\ 2.3 & 4.0 & 5.0 & 6.0 \end{bmatrix} \tag{22}$$

To validate the correctness and accuracy of the developed RNN-SVD for the computation of singular values, a general ill-conditioned matrix $\mathbf{G}$ has been considered to calculate its singular values. The accurate singular values can be obtained using $Matlab(2019b)$, which are 11.0072, 3.0123 and 0.4984. Ideally, several parameters of the developed RNN-SVD should be fine-tuned to work with data outside of the training set. Here, the initial parameters have been provided in Table 1. The left and right matrix columns $\mathbf{p}_j(0)$ and $\mathbf{q}_j(0)$ as inputs are randomly initialized with the normal distribution. It should be noted that the time step optimization is not considered in this example, which is used to purely demonstrate the correctness of RNN-SVD.

Table 1: Initial parameters of RNN-SVD for general matrix.

Δt_j	$E_{th}(j)$	$\mathbf{p}_j(0)$	$\mathbf{q}_j(0)$
0.01s	$1e^{-6}$	[-1.2074, 0.7172, 1.630]	[0.4888, 1.0346, 0.7268, -0.3034]

The comparison results of singular values and vectors decomposition have been shown in Table 2 and Fig. 4, where the good agreement between the physics-informed RNN-SVD and SVD by $Matlab$ has been observed. That means the developed RNN-SVD has the ability to obtain the singular values of general matrices with high accuracy. However, without considering the computational efficiency of SVD, the total number of iterations for the general matrix $\mathbf{G}$ is 938, which is much larger than the estimated 12 ($Iter <$

$4M$) of standard SVD method with randomly defined initials. It has been also noted that the converged left and right matrix columns during the SVD process are obviously different from the random initials shown in Fig. 4, indicating that the pre-trained initials could potentially improve the convergent speed. Therefore, to address the challenging initialization of the developed RNN-SVD, the time step optimization in Section 2.2.2 has been introduced in this example for the enhancement of the decomposition efficiency.

Table 2: Singular values of SVD and RNN-SVD.

	Order-1	Order-2	Order-3
SVD	11.00716783	3.01227636	0.49844497
RNN-SVD	11.00716783	3.01227636	0.49844482

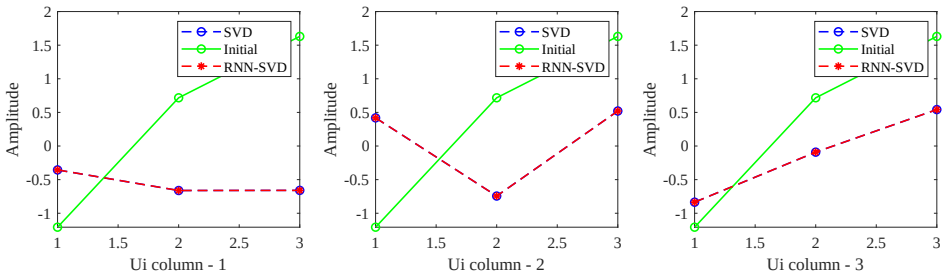

(a)

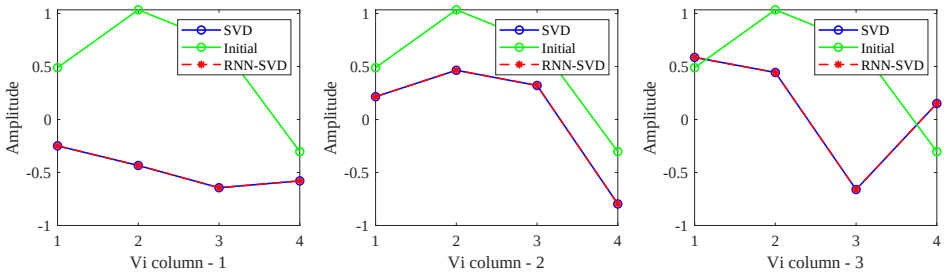

(b)

Fig. 4: Comparison of singular vectors results: (a) left singular vectors: $\mathbf{p}_j$, (b) right singular vectors: $\mathbf{q}_j$

As discussed in Section 2.2.2, the time step Δt_j and initial inputs $\mathbf{p}_j(0)$, $\mathbf{q}_j(0)$ have greatly influenced the convergent speed of RNN-SVD, it is vital to explore effects of the change of time steps on the performance of iteration loss. To demonstrate the convergent rate and sensitivity influenced by the time step Δt_j and initial inputs $\mathbf{p}_j(0)$, $\mathbf{q}_j(0)$, two studies shown in Fig. 5 have been conducted. First, five cases considering the variable Δt in the range of 0.01s to 0.05s have been investigated. Results have shown that

the convergent speed of RNN-SVD is getting faster with the increase of Δt. However, when $\Delta t = 0.05s$, the trend of the network convergence has suddenly changed to the divergence after 15 numbers of iterations, leading to the failure of satisfying the error threshold for a precise singular value. It is also worth noting that the loss gradients shown in the inset of Fig. 5(a) have gradually approached to the zeros after 20 numbers of iterations, indicating that the closer to the balance point is achieved, the loss variation is slower. Thus, more iterations have been required to reach the convergent results under the loss threshold. Based on these observations, influences of the change in the time step (Δt_{ratio}) on the loss function by the equation of $\Delta t(iter+1) = \Delta t(iter) + \Delta t(iter)/\Delta t_{ratio}$ have been illustrated in Fig. 5(b), when $\Delta t(0) = 0.01s$. It can be observed that the convergent speed has increased as Δt_{ratio} has become smaller in a certain range. Beyond that range, for example $\Delta t_{ratio} = 5$, the divergent behaviour of the iteration loss can be easily identified.

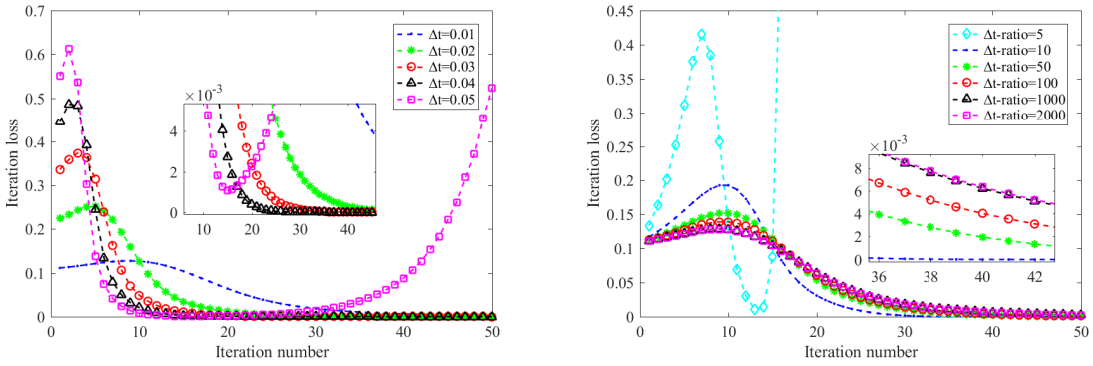

(a) (b)

Fig. 5: The convergent iteration number with different time steps: (a) constant Δt, (b) Δt with constant ratio.

Based on the discussions on results of the physics-informed RNN-SVD in terms of the time step and initial values of inputs, it is vital to choose the proper time step by adaptively changing its rate of change for the converged high-precision singular values with fewer iterations. It has been observed that the proper time step can effectively improve the convergent speed, which significantly contributes to the higher computational performance in the decomposition process over the standard SVD methods. Generally, the computational cost in the standard SVD process is exponentially increased as the rank of matrices becomes larger. Therefore, the more advantages of the developed RNN-SVD will be remarkably demonstrated by the higher-rank matrix that will be examined in the following section.

3.2. The Lumped-mass model validation

A three-degree-of-freedom lumped-mass model has been introduced to examine the pre-trained session and the time step optimization, which will promote the physics-informed RNN-SVD to effectively and precisely decompose the singular values and further identify the modal parameters. The lumped-mass model shown in Fig. 6 with the parameters defined by Eq. (23) have been used to conduct the natural frequency analysis. The acceleration response has been calculated by the ***Newmark-***β method. The time-dependent excitation force ($F(t) = 0.2 * sin(2\pi * 5 * t + \pi/4) + 0.1 * sin(2\pi * 7.5 * t + \pi/6)$) has been applied on the lumped mass 3. Moreover, 40db random noise has been added to the excitation force to stochastically simulate the practical environment condition. The acceleration responses of the lump mass 1 in the time and frequency domains have been shown in Fig. 7, where the first three modal frequencies of 0.799 Hz, 2.200 Hz and 3.303 Hz and the force frequency of 5 Hz have been clearly observed in the frequency domain. Based on these information, the effects of the pre-training session and adaptive time step optimization on computational costs have been investigated to explore the advances of the physics-informed RNN-SVD.

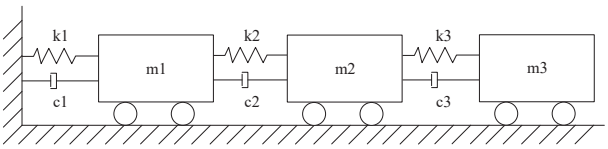

Fig. 6: A three-degree-of-freedom lumped-mass model.

$$\mathbf{K} = \begin{bmatrix} 960 & -450 & 0 \\ -450 & 1020 & -570 \\ 0 & -570 & 570 \end{bmatrix} \quad \mathbf{M} = \begin{bmatrix} 4.5 & 0 & 0 \\ 0 & 3.5 & 0 \\ 0 & 0 & 4 \end{bmatrix} \quad \mathbf{C} = \begin{bmatrix} 0.2 & -0.1 & 0 \\ -0.1 & 0.2 & -0.1 \\ 0 & -0.1 & 0.1 \end{bmatrix} \tag{23}$$

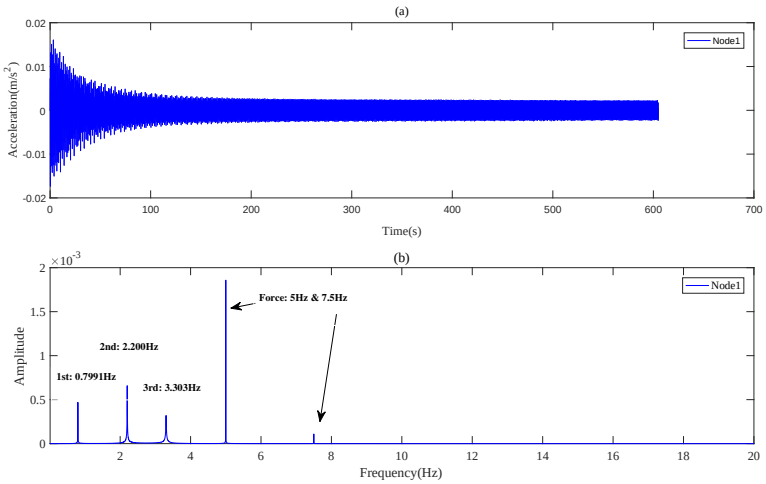

Fig. 7: The acceleration response of Node 1 by Newmark-beta method.

As described in Section 2.2.3, the decomposed-singular values the corresponding left and right matrices can be predicted in terms of the amplitude and sequence under the consideration of the similar external loading conditions. Therefore, the similar data patterns and features extracted from the system responses in the time and frequency domains can be observed in Fig. 7, where two segments have been selected from the acceleration response at the lumped mass 1. The sampling time for each segment is 60 seconds with the sampling rate of 50 Hz and the Hankel matrix is constructed with the rank of 1500. Two segments of signals in the time domain and their SVD results have been compared and shown in Figs. 8 and 9.

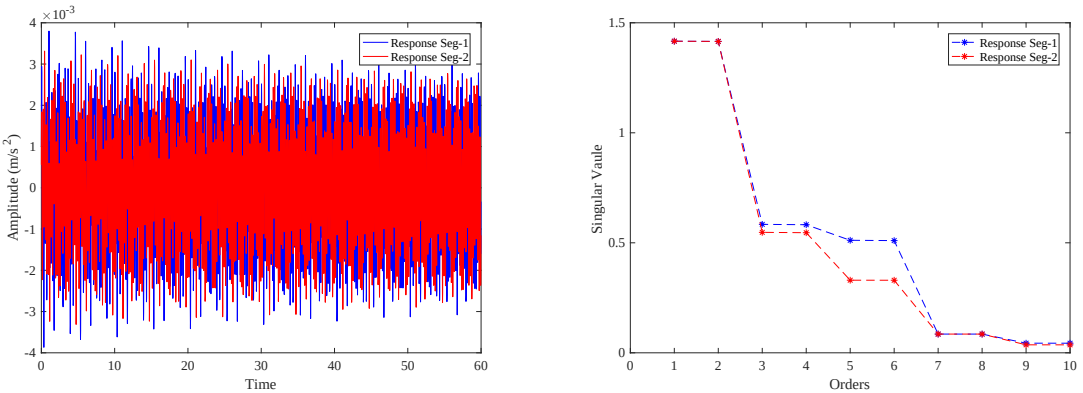

(a) (b)

Fig. 8: Two acceleration segments comparison: (a) time domain responses, (b) the singular values.

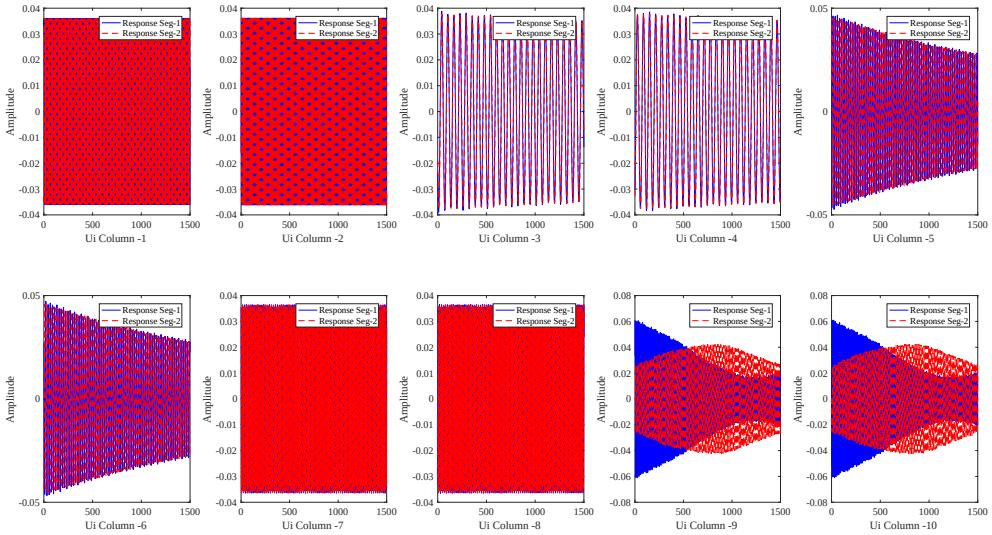

Fig. 9: Left matrix columns of two segments.

It has been noted that two segments (1 and 2) have been well agreed with each other in the time domain shown in Fig. 8(a), indicating the similar data pattern and feature of system responses. However, a slight discrepancy of the singular values between the orders in the range of 3 to 6 has been identified in Fig. 8(b) due to the energy difference of the intercepted two segments. In Fig. 9, remarkable results have shown the first eight columns in the left matrix during the SVD process have a high degree of similarity between two segments but the acceptable differences for the column-9 and column-10 can also be observed due to the random noise of the external force. Moreover, initial inputs of $\mathbf{p}_j(0)$ and $\mathbf{q}_j(0)$ can be selected from the existing results of SVD as the initializations of the investigated segment of the signal. Taking into account these situations, the development of the pattern matching strategy is quite necessary to mitigate the influence by random noise in the field monitoring case. Similarly, results in Fig. 9 have proved that the effectiveness of data pattern matching for improved computational performance of SVD can be achieved in pre-training processes using physics-informed RNN-SVD when multiple segments intercepted from the signal are available. Similarly, the time step should also be optimized to realize the high-efficiency computation of SVD. Based on these understanding, the developed RNN-SVD has adaptively utilized $\mathbf{p}_j$, $\mathbf{q}_j$ and singular values from Segment 1 as the inputs to identify the modal frequency of Segment 2. Considering there are only four frequency components in the system response, the first ten singular values should be decomposed due to the poles λ_n naturally presented as complex conjugate pairs. Also, the time step and its corresponding error

threshold have been pre-trained for each singular value to achieve a faster convergent speed. The time step optimization method defined by Eq. (21) with the initial time step $\Delta t_j(0)$, $\Delta t_{ratio}(j)$ and error thresholds values E_{th} has been provided in Table 3. Using these parameters, results of SVD for the response segment 2 have been shown in Figs. 10 and 11. It is worth noting that results by the physics-informed RNN-SVD have shown a good agreement with the solutions by the add-on SVD in $Matlab$. In terms of the computational efficiency, the numbers of iterations for the calculation of each singular value have been provided in Table 4. With the total number of 449 for the SVD computation, the physics-informed RNN-SVD has outperformed the standard SVD as it has required 1500*4 iterations to achieve the same results.

Table 3: The initial parameters of RNN-SVD.

Order	1	2	3	4	5	6	7	8	9	10
$\Delta t(0)$	0.3	0.3	0.35	0.4	0.4	0.4	0.5	0.5	0.5	0.5
Δt_{ratio}	2.5	2.5	4	2.85	3.33	3.33	1	1	0.95	0.86
E_{th}	$1e^{-4}$	$1e^{-4}$	$1e^{-4}$	$1e^{-4}$	$1e^{-4}$	$1e^{-4}$	$1e^{-5}$	$1e^{-5}$	$\mathbf{1e^{-5}}$	$\mathbf{1e^{-5}}$

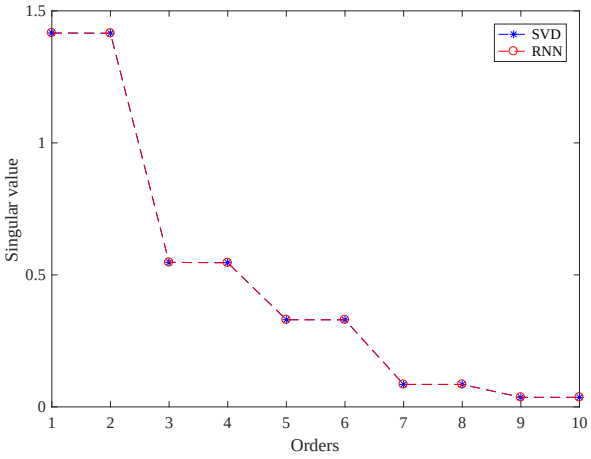

Fig. 10: The singular values comparison of SVD and RNN-SVD.

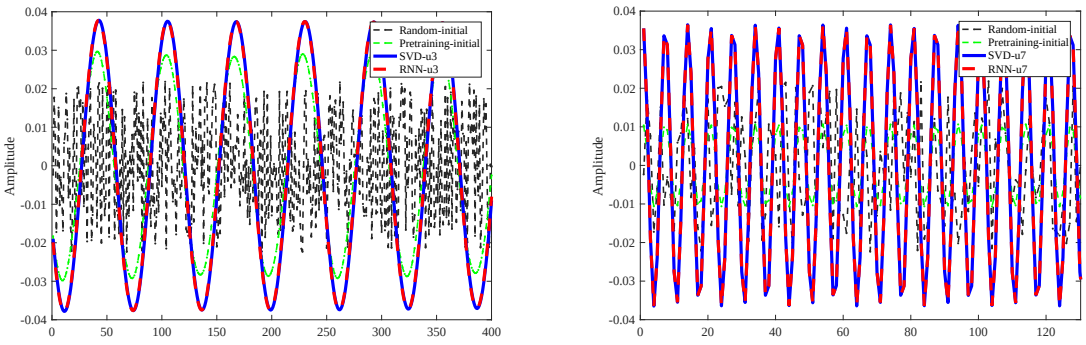

(a) (b)

Fig. 11: Left-columns comparison: (a) $\mathbf{p}_3$ (pre-training: 35 iterations; random: 5780 iterations), (b) $\mathbf{p}_7$ (pre-training: 29 iterations; random: 3362 iterations)

Table 4: The time consumption comparison.

	Order	1	2	3	4	5	6	7	8	9	10
RNN-SVD	iterations	4	5	35	34	23	35	29	23	157	104
	Time (10^{-2}s)	0.32	0.49	3.97	3.88	2.53	3.83	3.29	2.63	18.41	11.85
Time (s)	RNN-SVD	0.512									
	Randomized SVD (Minster et al., 2021)	0.885									
	Standard SVD	3.540									

To further demonstrate the advantage of RNN-SVD, the time consumption comparison with the standard SVD, that is to say, Eqs. (17) and (18) and a randomized SVD (Minster et al., 2021), has been provided in Table 4. The computational complexity of two methods are $4M$ and M (M represents matrix dimension), respectively. Meanwhile, in order to avoid the effect caused by the acceleration of matrix operation using different software platforms, the mean of matrix vector products (matvecs) is used as the base unit to measure the computation time by the standard SVD and randomized SVD. The average matvecs time is 0.00059 seconds and the mean time consumption of each iteration for RNN-SVD is 0.0011. The comparison results have indicated that the developed RNN-SVD has reduced up to six fold of computational time. Based on above SVD results, the modal frequencies of the system by Eqs. (3-7) can be obtained as 0.7991 Hz, 2.2008 Hz and 3.3061 Hz, when the developed RNN-SVD has converged with the MSE (Mean Square Error) value of $1.62e^{-6}$. Meanwhile, it has been noted that initial columns obtained in the pre-training ses-

sion have significantly increased the convergent speed and the result accuracy as compared with the random initial in Fig. 11(a) and (b), leading to the reduction of the number of iterations, for example, from 5780 to 35 for $\mathbf{p}_3$ and from 3362 to 29 for $\mathbf{p}_7$. However, there has been a slight discrepancy between SVD results by pre-training and the physics-informed RNN-SVD. This is mainly caused by the different singular values of two segments depicted by Line 11 in $Algorithm2$. As it is hardly to find two identical segments in the practical monitoring process, the non-overlap of two curves representing SVD computations can not be avoided, but minimized by the implementation of pre-training session into the network. The final results have proved that there is in excellent agreement between singular values obtained by the proposed method and $Matlab$. In conclusion, numerical results have showed that the time step optimization and data pattern learning of inputs can effectively promote the physics-informed RNN-SVD with the remarkably reduced computational burden in the SVD process.

4. Field data study

The numerical studies in Section 3 have proved the computational effectiveness and efficiency of the proposed framework and its adaptivity in vibration feature extractions including singular values and modal frequencies. As a representative example, the study on field data from an in-service OWT has been conducted to further validate the correctness of the proposed framework for performance monitoring of the structure subject to the time-varying environmental and operational to explore the feasibility for adaptive real-time monitoring. The field data has been collected from a real-time monitoring system deployed in a mono-pile OWT structure in Yellow sea of Rudong (121°26.5'E, 32°47.6'N, Jiangsu, China) as shown in Fig. 12. And the real-time monitoring procedures have been shown in Fig. 13.

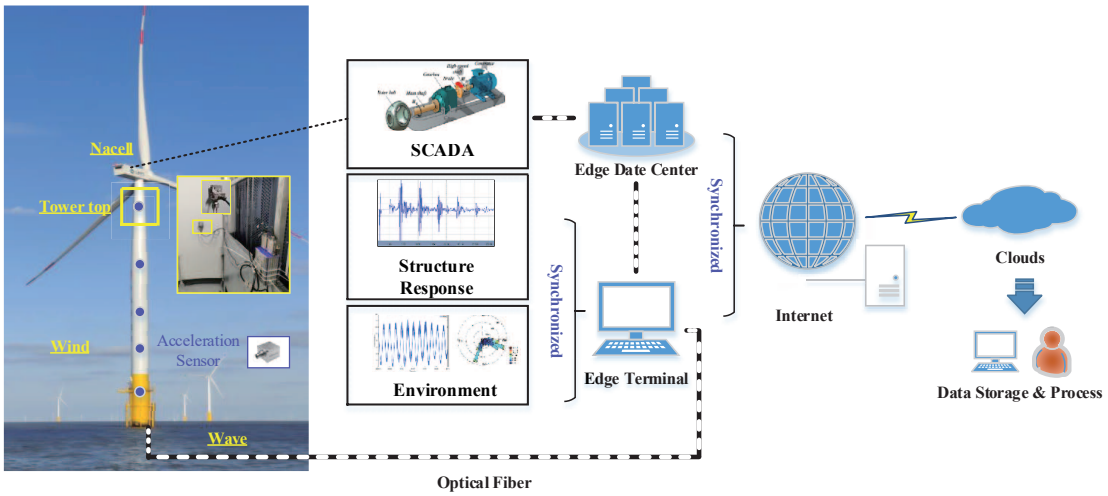

Fig. 12: Field monitoring system framework.

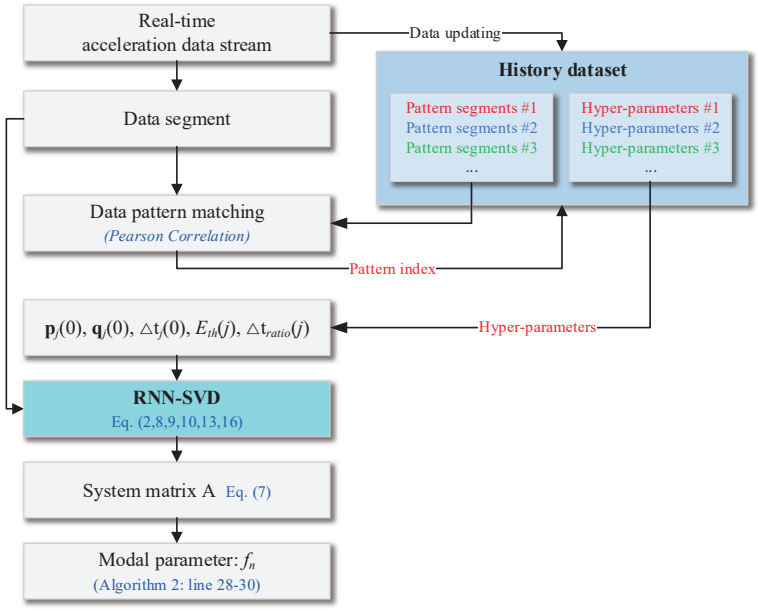

Fig. 13: Real-time monitoring flow chart.

4.1. Field data pattern matching

As discussed in Section 2.2.4, to ensure the identification of the selected data patterns and features from streaming measurements in the pre-training session, the history dataset and representative data patterns should be well prepared in advance by the offline learning with optimal hyper-parameters. Generally, the structural vibration performance will vary with the structure state and the time-varying external loads. Here,

three typical stable states which frequently appear in the operational periods and their associated wind loads and rotor speeds have been listed in Table 5. As the structure acceleration response, wind speed and the rotor speed data (SCADA) are synchronously collected in Fig. 14, the acceleration data can be observed to behave quite different with the varying environmental and operational conditions. In fact, the rotor speed is more obvious to present the operational status of OWT, which can be evidenced as the stable indicators, e.g., data pattern 1-3 labelled in Fig. 14(c).

Table 5: The three data patterns*.

	Data pattern 1 (parking)	Data pattern 2 (low speed)	Data pattern 3 (rated speed)
Wind speed (m/s)	1-2	3-4	9-10
Rotor speed (r/min)	0-0.15	6.5	11.2

*Each data pattern segment includes 3000 sampling points.

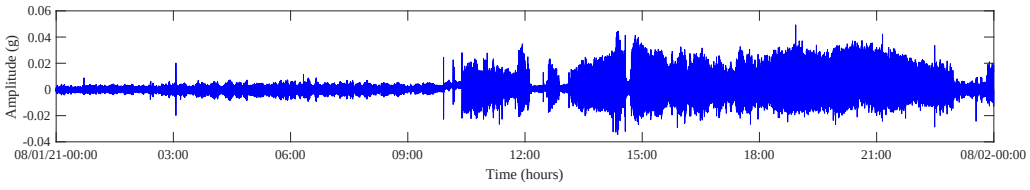

(a)

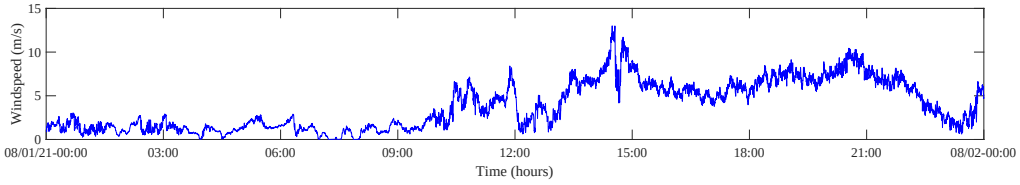

(b)

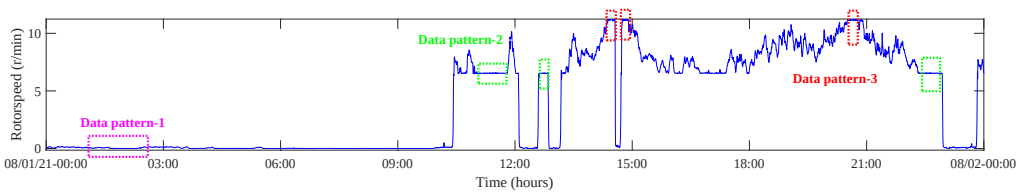

(c)

Fig. 14: The synchronized data of monitoring system: (a) acceleration data, (b) wind data, (c) rotor data

To emphasize the importance of data pattern and feature learning in the pre-training session, four typical operational conditions of OWT shown in Fig. 15 have been considered for structural analysis in terms of the frequency and singular values. It has been worth noting that the results are remarkably different, indicating the vital significance on the selection of appropriate data patterns and features for efficient and effective computations in the practical applications of the proposed framework. As discussed in Section 2.2.3, the rule of thumb for the selection of data patterns should aim at the segments of signals reflecting a relatively stable state for the avoidance of additional errors and fluctuations in the feature matching process. As the energy proportion of the first modal component in the vibration response should be comparatively larger than other components and noise in the segment for the selected data pattern learning, the few orders need to be extracted using the physics-informed framework for the realization of a more efficient system identification.

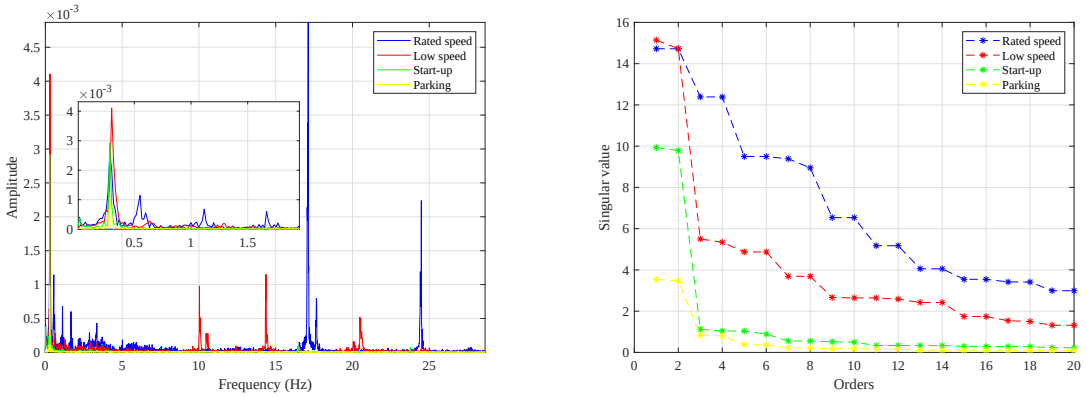

(a) (b)

Fig. 15: The comparison of acceleration data in four operational conditions: (a) frequency domain, (b) singular values.

As mentioned in $Algorithm2$, the *Pearson-correlation* has been used as the criterion to judge the degree of matching between the selected data patterns and the streaming monitoring signal. In this study, the streaming data on August 1^{st} have been selected to calculate the coefficients of three referenced data patterns that have been labelled in Fig. 16. It should be noted that only the highly correlated streaming segments (data patterns 1 and 3: coefficient > 0.94; data pattern 2: coefficient > 0.8) have been marked with different symbols. It can be observed that the environmental and working conditions for segments with high coefficients are very close to the load conditions for the selected data patterns in Table 5. This has proved that the Pearson-correlation can be applied to effectively measure the matching of data patterns. Moreover,

a more trustworthy coefficient threshold should be defined to reflect the degree of data pattern matching from the long-term monitoring data. Thus, the data from August 1^{st} to 7^{th} in Fig. 17 has been used to statistically determine the suitable coefficient threshold based on its distribution under wind and rotor speed conditions. Results have shown that the coefficient distributions of data patterns 1 and 3 are distinguishably separable when the coefficient threshold is set above 0.94. Similarly, the matching between the streaming signal and data pattern 2 can be judged when the threshold is larger than 0.85. In summary, under the wind and rotor speed conditions in Table 5, the threshold values of three data patterns for measuring the match degree have been set as 0.94, 0.85 and 0.94, respectively.

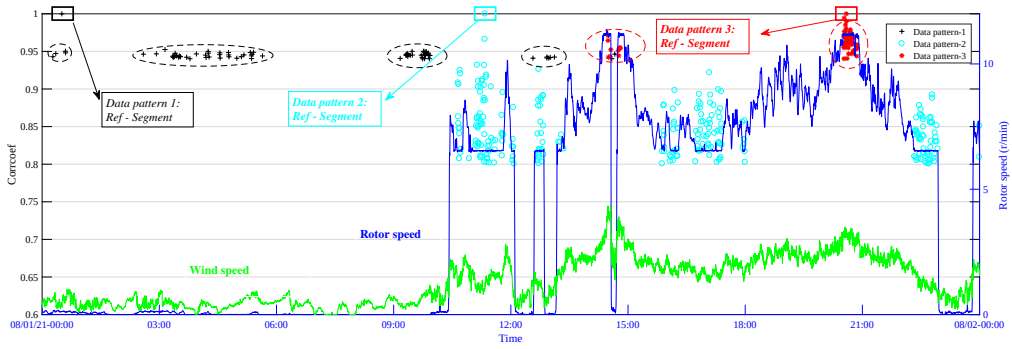

Fig. 16: The correlation coefficients of the three data pattern on August 1^{st}.

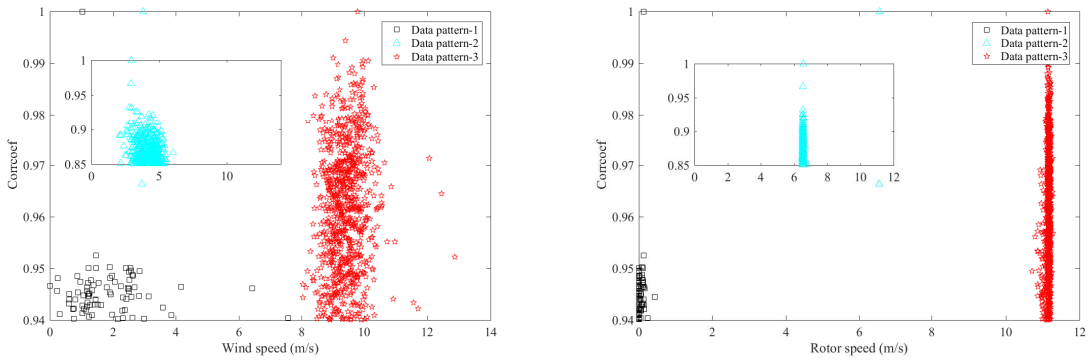

(a) (b)

Fig. 17: The coefficient distribution of three data patterns in seven days: (a) wind speed, (b) rotor speed

It has been worth noting that the threshold value for data pattern 2 is comparatively lower than values for the other two patterns, thus only the data patterns 1 and 3 have been considered for SVD computations and the first modal frequency identification. Once the corresponding input initial conditions are obtained

by the pre-trained using the referenced data segments, adaptively identify modal parameters with a higher level of computational efficiency will be achieved by the proposed RNN-SVD. The initial inputs of the first eight orders for two data patterns have been listed in Table 6.

Table 6: The initial parameters of two data patterns .

		Singular value orders							
		1	2	3	4	5	6	7	8
Data pattern 1	$\Delta t(0)$	0.31	0.3	0.3	0.3	0.3	0.4	0.4	0.3
	Δt_{ratio}	0.9	0.9	0.9	1.5	1.5	2	2	2
	E_{th}	$1e^{-4}$	$1e^{-4}$	$1e^{-4}$	$1e^{-4}$	$1e^{-4}$	$1e^{-4}$	$1e^{-5}$	$1e^{-5}$
Data pattern 3	$\Delta t(0)$	0.02	0.1	0.1	0.1	0.1	0.15	0.15	0.2
	Δt_{ratio}	0.1	0.15	0.15	0.15	0.15	0.15	0.15	0.2
	E_{th}	$1e^{-5}$	$1e^{-5}$	$1e^{-5}$	$1e^{-5}$	$1e^{-5}$	$1e^{-5}$	$1e^{-5}$	$1e^{-5}$

4.2. The 1^{st} modal frequency identification

Considering that data patterns and initial inputs have been obtained in Section 4.1, two groups of streaming data (three segments in each group) in the range of August 1^{st} to 7^{th} have been used for the modal identification analysis by the proposed framework described in $Algorithm2$. The comparison results of time consumption and the first modal frequency have been provided in Table 7.

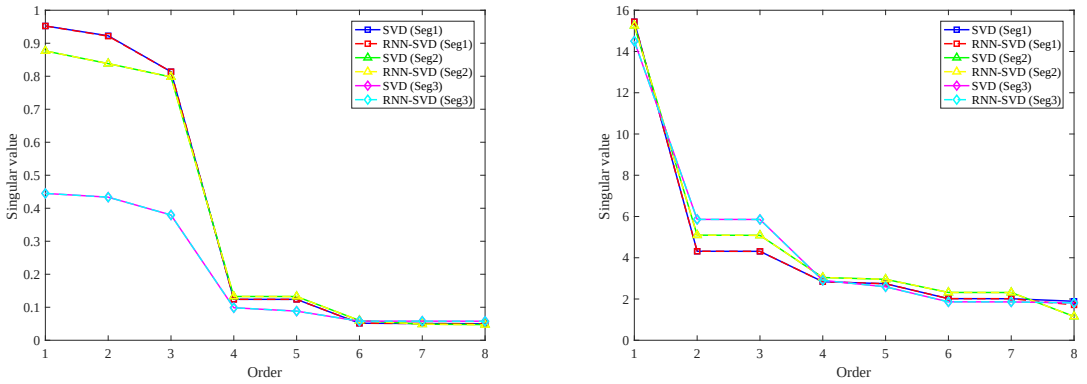

(a) (b)

Fig. 18: The singular value comparison results of RNN-SVD and SVD ($Matlab$): (a) data pattern 1 (parking), (b) data pattern 3 (rated speed)

Table 7: The comparison results of time consumption and 1^{st} modal frequency.

		Data pattern 1			Data pattern 3		
		Seg-1	Seg-2	Seg-3	Seg-1	Seg-2	Seg-3
RNN-SVD	Iteration numbers	1312	916	1170	491	394	788
	Time consumption (s)	**2.094**	**1.300**	**1.820**	**0.560**	**0.420**	**0.850**
Randomized SVD: time consumption (s)		**0.9315**	**0.9214**	**0.9179**	**0.9306**	**0.9545**	**0.9440**
Standard SVD: time consumption (s)		**3.726**	**3.6856**	**3.6717**	**3.7226**	**3.818**	**3.776**
1^{st} frequency (Hz)	ERA	0.2735	0.2797	0.2765	0.2806	0.2856	0.2844
	Propsoed framework	**0.2735**	**0.2766**	**0.2785**	**0.2806**	**0.2856**	**0.2847**

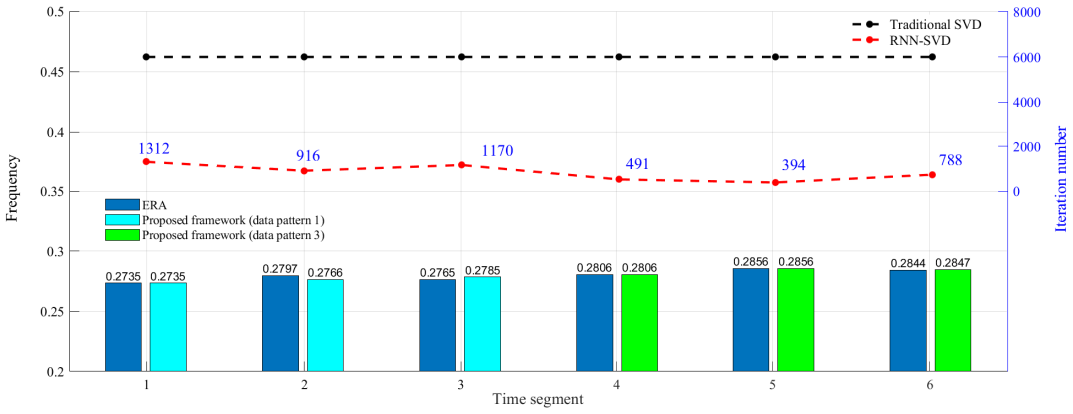

Fig. 19: A comprehensive illustration of results obtained by the proposed framework and ERA.

Results in Fig. 18 have showed that the proposed framework has the ability to precisely realize the singular values decomposition of the structure responses and successfully achieved the identification of two different patterns. In Table 7, the time consumption of RNN-SVD has been remarkably reduced as compared with the results by the standard method, especially in the case of data pattern 3. With the comparison of the randomized SVD, the RNN-SVD has the computational advantage in the pattern 3 case and a slight different level of time cost in the case of pattern 1 as the data in the pattern 3 is more stable than in the pattern 1. This example has provided the evidence that the data pattern selection and initial parameters setting determine the efficiency of RNN-SVD in the real-time monitoring of the complex engineering system. With the improved history dataset, the data patterns and hyper-parameters can be more efficiently selected

to leverage the developed framework in the monitoring process of the engineering structures. The comparison result of the first frequency has revealed that the physics-informed framework has the great capability to guarantee the same level of computational accuracy as ERA, especially better performances including the convergent speed and the precision of the first frequency for the identification of data pattern 3. A comprehensive illustration of main results to demonstrate the outperformance of the proposed framework over the traditional methods in terms of the iteration number and the first frequency have been presented in Fig. 19. It has been worth noting that the small difference of singular values calculated by both the proposed framework and $Matlab$ has further proved the correctness and accuracy of RNN-SVD in Fig. 18. Moreover, data pattern 3 represents a more stable state than the other two patterns by the evidence demonstrating the overlap of three segment curves in the data pattern 3. Therefore, the responses under the rated speed operation, that is the feature represented by the data pattern 3 shown in Table 5, should be considered a characteristic of the system in the real monitoring process. In conclusion, it has been proved that the physics-informed modal identification framework has effectively enabled the realization of efficient monitoring suitable for practical engineering applications.

5. Conclusion

In this paper, a novel physics-informed framework to realize an adaptive, computationally efficient and accurate modal identification method has been proposed for real-time adaptive monitoring of offshore structures. The innovative design of the proposed framework is converting the modal identification principle into an optimal SVD process governed by differential equations via the RNN-SVD network. The correctness and computational efficiency have been demonstrated by two numerical studies in which the time consumption has been reduced from 3.5504 seconds (standard SVD) to 0.512 seconds (RNN-SVD). The eminent challenges of the random input initialization and time-increment factor for the network have been successfully addressed by the pattern matching strategy and adaptive time step optimization, respectively. Consequently, three referenced data patterns of an in-service OWT structure for parking, low and rated speeds have been identified by the pre-defined threshold indexes of 0.94, 0.85 and 0.94, respectively. And the 1^{st} frequency from the selected data segments has been efficiently and precisely identified, leading to an accurate real-time monitoring for OWT structure.

Throughout above studies, the limitations of the proposed framework have been summarized as following two aspects:

1. Pre-training input parameters of the proposed framework could lead to the poor generalization performance due to the over-fitting of data.

2. The computational performance of the proposed method would be compromised by the weak mode data as the decomposition order is increased.

For the further exploration, the proposed method is expected to construct a meaningful framework for the development of real-time smart technology applicable to a broad range of SVD-related sciences such as modern monitoring, dimension reduction and signal processing.

6. Declaration of competing interest

The authors declare that they have no known competing financial interests or personal relationships that could have appeared to influence the work reported in this paper.

7. Acknowledgements

The authors acknowledge the financial support of the National Outstanding Youth Science Fund Project of National Natural Science Foundation of China (52125106) and the National Natural Science Foundation project (U22A20243). Thanks to China Green Development Group, Rudong offshore wind farm in Jiangsu Province and Power China Huadong Engineering Corporation Limited, for their strong support on the field monitoring system test in this paper.

References

Ahmad, S., Lavin, A., Purdy, S., Agha, Z., 2017. Unsupervised real-time anomaly detection for streaming data. Neurocomputing 262, 134–147. doi:10.1016/j.neucom.2017.04.070.

Avci, O., Abdeljaber, O., Kiranyaz, S., Hussein, M., Inman, D.J., 2021. A review of vibration based damage detection in civil structures: from traditional methods to machine learning and deep learning applications. Mechanical Systems and Signal Processing 147, 107077. doi:10.1016/j.ymssp.2020.107077.

Bao, X., Shi, C., 2019. Ambient vibration responses denoising for operational modal analysis of a jacket-type offshore platform. Ocean Engineering 172, 9–21. doi:10.1016/j.oceaneng.2018.11.040.

Bao, Y., Li, H., 2020. Machine learning paradigm for structural health monitoring. Structural Health Monitoring 20, 1353–1372. doi:10.1177/1475921720972416.

Choe, D.E., Kim, H.C., Kim, M.H., 2021. Sequence-based modeling of deep learning with lstm and gru networks for structural damage detection of floating offshore wind turbine blades. Renewable Energy 174, 218 – 235. doi:10.1016/j.renene.2021.04.025.

Cichocki, A., 2002. Neural network for singular value decomposition. Electronics Letters 28, 784–786. doi:10.1049/el:19920495.

Devriendt, C., Magalhaes, F., Weijtjens, W., Sitter, G.D., Cunha, A., Guillaume, P., 2014. Structural health monitoring of offshore wind turbines using automated operational modal analysis. Structural Health Monitoring 13, 644–659. doi:10.1177/1475921714556568.

Dong, X., Lian, J., Wang, H., Yu, T., Zhao, Y., 2018. Structural vibration monitoring and operational modal analysis of offshore wind turbine structure. Ocean Engineering 150, 280–297. doi:https://doi.org/10.1016/j.oceaneng.2017.12.052.

Erhan, L., Ndubuaku, M., Di Mauro, M., Song, W., Chen, M., Fortino, G., Bagdasar, O., Liotta, A., 2021. Smart anomaly detection in sensor systems: A multi-perspective review. Information Fusion 67, 64–79. doi:10.1016/j.inffus.2020.10.001.

Facchini, L., Betti, M., Biagini, P., 2014. Neural network based modal identification of structural systems through output-only measurement. Computers and Structures 138, 183–194. doi:10.1016/j.compstruc.2014.01.013.

Fang, N., Zhou, Y., Ye, Q., Li, Y., 2017. Modal parameter identification of vibration signal based on unsupervised learning convolutional neural network. Journal of Computer Applications 37, 786–790, 822.

Feijo, M., Zambrano, Y., Vidal, Y., Tutivn, C., 2021. Unsupervised damage detection for offshore jacket wind turbine foundations based on an autoencoder neural network. Sensors 21, 3333. doi:10.3390/s21103333.

Feng, D., Bao, Z., Jiao, L., 1995. A left-right nueral network for singularvalue decompositions of general matrices. ACTA Electronica SINCA 23, 115–118.

Feng, D., Bao, Z., Jiao, L., 1997. A new total parallel neural network for svd. Journal of Electronics and Information Technology 19(1), 17–23.

Flah, M., Nunez, I., Chaabene, W.B., Nehdi, M.L., 2021. Machine learning algorithms in civil structural health monitoring: A systematic review. Archives of Computational Methods in Engineering 28, 2621–2643. doi:10.1007/s11831-020-09471-9.

Hu, S., Yang, W., Li, H., 2013. Signal decomposition and reconstruction using complex exponential models. Mechanical Systems and Signal Processing 40, 421–438. doi:10.1016/j.ymssp.2013.06.037.

Ibrahim, S.R., Mikulcik, E.C., 1977. A method for the direct identification of vibration parameters from the free response. Shock and Vibration Bulletin .

James, G., Carne, T., Laufer, J., 1995. The natural excitation technique (next) for modal parameter extraction from operating structures. The International Journal of Analytical and Experimental Modal Analysis 10.

Juang, J., Pappa, R., 1985. An eigensystem realization algorithm for modal parameter identification and model reduction. Journal of Guidance Control and Dynamics 8, 620–627. doi:10.2514/3.20031.

Lam, X., Mevel, L., 2011. Uncertainty quantification for eigenvalue-realization-algorithm, a class of subspace system identification. IFAC Proceedings Volumes 44, 6529–6534. doi:10.3182/20110828-6-IT-1002.00619.

Lei, L., Gang, Y., Jing, G., 2022. Physics-guided neural network for underwater glider flight modeling. Applied Ocean Research 121, 103082. doi:https://doi.org/10.1016/j.apor.2022.103082.

Liao, D., Zhu, S.P., Correia, J.A., De Jesus, A.M., Veljkovic, M., Berto, F., 2022. Fatigue reliability of wind turbines: historical perspectives, recent developments and future prospects. Renewable Energy 200, 724–742. doi:10.1016/j.renene.2022.09.093.

Liu, F., Li, H., Lu, H., 2016. Weak-mode identification and time-series reconstruction from high-level noisy measured data of offshore structures. Applied Ocean Research 56, 92–106. doi:10.1016/j.apor.2016.01.001.

Lu, Y., Sun, L., Zhang, X., Feng, F., Kang, J., Fu, G., 2018. Condition based maintenance optimization for offshore wind turbine considering opportunities based on neural network approach. Applied Ocean Research 74, 69–79. doi:https://doi.org/10.1016/j.apor.2018.02.016.

Luo, C., Keshtegar, B., Zhu, S.P., Niu, X., 2022a. Emcs-svr: Hybrid efficient and accurate enhanced simulation approach coupled with adaptive svr for structural reliability analysis. Computer Methods in Applied Mechanics and Engineering 400, 115499. doi:10.1016/j.cma.2022.115499.

Luo, C., Keshtegar, B., Zhu, S.P., Taylan, O., Niu, X.P., 2022b. Hybrid enhanced monte carlo simulation coupled with advanced machine learning approach for accurate and efficient structural reliability analysis. Computer Methods in Applied Mechanics and Engineering 388, 114218. doi:10.1016/j.cma.2021.114218.

Mao, J., Wang, H., Spencer, B.F., 2020. Toward data anomaly detection for automated structural health monitoring: Exploiting generative adversarial nets and autoencoders. Structural Health Monitoring 20, 1609–1626. doi:10.1177/1475921720924601.

Minster, R., Saibaba, A., Kar, J., Chakrabortty, A., 2021. Efficient algorithms for eigensystem realization using randomized svd. Society for Industrial and Applied Mathematics 42, 1045–1072. doi:https://doi.org/10.48550/arXiv.2003.11872.

Oja, E., 1982. A simplified neuron model as a principal component analyzer. Journal of Mathematical Biology 15, 267–273. doi:10.1007/BF00275687.

Olivieri, C., Paulis, F.D., Orlandi, A., Pisani, C., Giannuzzi, G., Salvati, R., Zaottini, R., 2020. Estimation of modal parameters for inter-area oscillations analysis by a machine learning approach with offline training. Energies 13, 6410. doi:10.3390/en13236410.

Peeters, B., De Roeck, G., 1999. Reference-based stochastic subspace identification for output-only modal analysis. Mechanical Systems and Signal Processing 13, 855–878. doi:https://doi.org/10.1006/mssp.1999.1249.

Puruncajas, B., Vidal, Y., Tutivn, C., 2020. Vibration-response-only structural health monitoring for offshore wind turbine jacket foundations via convolutional neural networks. Sensors 20, 3429. doi:10.3390/s20123429.

Qin, M., Chen, H., Zheng, R., Gao, T., 2021. An adaptive operational modal analysis method using encoder lstm with random decrement technique. Journal of Sensors doi:10.1155/2021/7199888.

Qiu, B., Lu, Y., Sun, L., Qu, X., Tong, F., 2020. Research on the damage prediction method of offshore wind turbine tower structure based on improved neural network. Measurement 151, 107141–. doi:10.1016/j.measurement.2019.107141.

Schmidt, R.M., 2019. Recurrent neural networks (rnns): A gentle introduction and overview doi:10.48550/arXiv.1912.05911, arXiv:1912.05911.

Su, L., Huang, X., Song, M.L., LaFave, J., 2020. Automatic identification of modal parameters for structures based on an uncertainty diagram and a convolutional neural network. Structures 28, 369–379. doi:10.1016/j.istruc.2020.08.077.

Teng, D., Feng, Y., Chen, J.Y., Lu, C., 2022. Structural dynamic reliability analysis: review and prospects. International Journal of Structural Integrity 13, 753–783. doi:10.1108/IJSI-04-2022-0050.

Torbol, M., Park, K.T., 2018. Machine learning and digital image processing for non-contact modal parameters identification of structures, in: Sensors and Smart Structures Technologies for Civil, Mechanical, and Aerospace Systems. doi:10.1117/12.

2299329.

Weijtjens, W., Verbelen, T., Sitter, G.D., Devriendt, C., 2016. Foundation structural health monitoring of an offshore wind turbine: a full-scale case study. Structural Health Monitoring 15, 389–402. doi:10.1177/1475921715586624.

Worden, K., Green, P.L., 2017. A machine learning approach to nonlinear modal analysis. Mechanical Systems and Signal Processing 84, 34–53. doi:10.1016/j.ymssp.2016.04.029.

Yao, Y., Yang, Y., Wang, Y., Zhao, X., 2019. Artificial intelligence-based hull structural plate corrosion damage detection and recognition using convolutional neural network. Applied Ocean Research 90, 101823. doi:https://doi.org/10.1016/j.apor.2019.05.008.

Yuan, F., Zargar, S.A., Chen, Q., Wang, S., 2020. Machine learning for structural health monitoring: challenges and opportunities. Sensors and Smart Structures Technologies for Civil, Mechanical, and Aerospace Systems 11379, 1–23. doi:10.1117/12.2561610.

Zhou, L., Li, Y., Liu, F., Jiang, Z., Yu, Q., Liu, L., 2019. Investigation of dynamic characteristics of a monopile wind turbine based on sea test. Ocean Engineering 189, 106308. doi:10.1016/j.oceaneng.2019.106308.